Iran University of Science and Technology

Dynamic Modeling and Active Control of Slip Phenomenon in a Four-axle Locomotive

H. Molatefi [1*], I. Ferestade [1], N. Taefi Aghdam[2]

[1]School of Railway Engineering, Iran University of Science and Technology, Tehran, Iran

[2]School of Mechanical Engineering, Tarbiat Modares University, Tehran, Iran

ARTICLE INFO	ABSTRACT
	Nowadays, active control of rail vehicles, wheel slip control, in particular, is of great importance. Regarding the various methods of slip control, selecting the best method is necessary for the design of rail vehicles. In this paper, first, a slip simulator for a four-axle locomotive was selected to simulate the slip phenomenon; then, components of this simulator were separately designed, and finally, its 3D model was presented. Afterward, dynamic equations were derived based on nonlinear creep theory for this simulator, and the dynamic modeling of the slip was obtained through solving state-space equations. Using fuzzy control with three different methods, per vehicle, per bogie, as well as per wheelset, the controller was designed, and finally, the best approach for controlling the slip was determined by adding this controller to the dynamic model.

1. Introduction

By considering the importance of the slip phenomenon control in locomotives, as well as the existence of different methods for the slip control in rail vehicles, evaluation of these approaches and selection of the optimum case is very significant in the railway industry. Since, for the assessment of the methods, a realistic model is needed and also considering that this model design and development is costly and time-consuming, thus, at the first step designing a dynamic mathematical model is necessary for the slip phenomenon. After these steps, designing and developing the real simulator based on the mentioned dynamic model is essential to investigate different approaches of slip control and select the best.

Kim et al. [1] in 1999 applied an electromechanical simulator to examine the slip control. To control slip in this simulator first, the adhesive force between wheel and rail was estimated using an observer, and eventually, it

was tried to maintain this force at the maximum value.

Wilson et al. [2] used the mechatronic theory for the simulation and the control of slip. In this method, a mechatronic model of the wheels and axle were used in order to simulate the slip; its details are presented in [2]. Moreover, Park et al. [3] in 2001 employed the engine parallel control method for controlling the adhesion in the wheel-rail contact in high-speed trains. Experimental analysis of the adhesion between wheel and rail with the use of a real scale model was carried out by Zhang et al. [4] in 2002. Yamazaki et al. [5] in 2005, used the slip control method through a real scale simulation, and Holmet et al. [6] in 2008, conducted a simulation for the slip control using a virtual sample for the electric locomotive. Smejkal et al. [7] in 2014 developed a simulator to check adhesion between wheel and rail in different contact conditions. Given that the purpose of this instrument is to examine adhesion between wheels and rails in different conditions of rail.

---

*Corresponding author, Associate professor
Email: molatefi@iust.ac.ir

Bosso et al. [8] in 2015 suggested a new simulator that can examine the effect of multi-axis in the tests after considering the limitations of a single-axle simulator. Naeimi and Li [9] in 2016 introduce the dynamic analysis of a test rig, in order to assess the vibration behavior of the system with respect to contact phenomenon.

According to the simulation models offered and the characteristics of each, in this paper, the same simulator model of Kim [1] was used. This model can model the performance of the four-axle locomotives in more working conditions since it has four discs, while the ones built based on a single disc have many restrictions. These limitations include the inability of these models in the implementation of different control algorithms. In the simulators with a single disc, the control system can handle only the simulator disc; in other words, in such simulators, only control algorithms for each axle can be examined. However, in the simulator with four discs, the control goal can be changed from all axles' control (control of all four wheels simultaneously) to the bogie control (control of two discs simultaneously), as well as control of each axle (control of each disc separately) by changing the control method.

Given that the slip control methods are different in different trains, it is possible to review and compare all these methods via this simulator. Furthermore, a single disc simulator cannot be used in the difference of friction conditions for the front and rear wheels of four-axle locomotives as these simulators do not have the modeling capabilities in such circumstances. In the simulators with four discs, linear velocity locomotive can also be determined while in one disc simulator, the parameter cannot be estimated due to one disc. Unfortunately, despite the model proposed by Kim et al. [1] takes four discs, the features listed are not included well for the simulator. Besides, Kim's proposed model is designed just for the terms of acceleration, and the slip analysis in braking is not included in the simulator.

In this paper, a simulator is introduced, which can regard the various slip control algorithms, and it is designed to consider different conditions of rail for four-axle locomotives. First, all separate components of this simulator were designed, and its 3D model was presented. Then, the dynamic equations of the simulator were determined and solved through the Runge-Kutta

4th order method in MATLAB. Finally, for the active control of the system and selection of the best controlling method, the fuzzy control method with three different mechanisms was used.

2. Electromechanical Simulator

The electromechanical simulator has four small discs driven by four induction motors, in contact with four large discs, representing the contact model of the wheel and rail. Each of these small discs represents an axle of a rail vehicle. The large discs are mounted on a large axle; the linear speed of this axle represents the linear speed of the rail vehicle. To apply normal force between the wheel and the rail, a power screw is used, so that by closing and opening this screw, reasonable force between wheel and rail is set. The simulator dimensions are shown in Table 1 [1].

Table 1. Dimensional characteristics of the slip simulator [1]

Induction motor	Rated output power	0.75 (kW)
	Number of poles	4
	Rated output torque	4.1 (Nm)
Small wheel for train wheel	Diameter(d)	0.12 (m)
	Width(l)	0.025 (m)
Large wheel for train body	Diameter(D)	0.6 (m)
	Width(L)	0.018 (m)
Shaft for large wheel	Diameter(a)	0.2 (m)
	Length(T)	0.3 (m)
gear	Not used	

In the following, the design trend of other components of the simulator is described.

2.1. Designing simulator components

2.1.1. Bearing design

After reviewing the advantages and disadvantages of different types of bearings, it can be concluded that the roller bearings are more appropriate. For the final selection of the bearing, calculations of the roller bearings according to DIN 622 is being taken. Prior to the calculation of the lifetime of the roller bearings, the equivalent load are calculated with respect to the effective force on the bearings. For the roller bearings with the radial load of F_r and the axial load of F_a and with the radial and axial

coefficients of x and y respectively, the equivalent load would be achieved [10]:

$$P = xF_r + yF_a \qquad (1)$$

The relationship between the dynamic transmission coefficient with the lifetime and load of the roller bearings in million rounds as follows [9]:

$$L = (\frac{C}{P})^3 = \frac{60L_h n}{10^6} \qquad (2)$$

To obtain the lifetime, first, the dynamic transmission coefficient must be obtained using factors of heat, f_t; the number of rounds, f_n; and lifetime, f_L through the following equation [10]:

$$c = P \frac{f_L}{f_n f_t} \qquad (3)$$

This way, using the obtained dynamic transmission coefficient, the desired bearing diameter, as well as tables in [10], the appropriate bearing can be selected. In this process, the dynamic transmission coefficient of the selected bearing should be greater than or equal to the obtained value.

Finally suitable bearings considering the tables in [10] are determined as follows:

- Deep groove ball bearings 6016 based on DIN 625 with the dynamic transmission coefficient of 3750

- Deep groove ball bearings 6216 based on DIN 625 with the dynamic transmission coefficient of 5700

- Two-sided angular contact ball bearings 6016 based on DIN 628 with the dynamic transmission coefficient of 4000

- Cylindrical roller bearings NU 10 16 based on DIN 5412 with the dynamic transmission coefficient of 6000

2.1.2. Axle design

Carrier axles of machines are a rotating part of them, including pulleys of fan belt wheels, gears, motion wheels, and reel. In normal cases, axles and shafts are made of either steel S275JR (St44-2) or E295 (St 50-2), and in the case of being under the severe tensions, they are made of steel E335 (St 60-2); for this, the steel E335 is chosen for the axle.

2.1.2.1. Calculating the axle diameter

In the design of the axle, when it at different operating conditions transmits power, the proper diameter of the axle primarily should be determined such that its strength and rigidity to be satisfactory. Further, in this design, flexural and torsional moments seems to be among the effective factors. Regulation of the American Society of Mechanical Engineers suggests the following equation for designing the diameter of a hollow axle. In this relation, the effects of the flexural and torsional loads, as well as shock and fatigue factors, are considered [10]:

$$d_o^3 = \frac{16}{\pi S_s (1 - K^4)} \sqrt{(k_b M_b)^2 + (k_t M_t)^2} \qquad (4)$$

Where S_s for axles without any place for grooves and those with places for grooves are equal to $55 \frac{N}{mm^2}$ and $40 \frac{N}{mm^2}$, respectively [10]. Therefore, according to (4), axle diameter is calculated to be 30.5 mm after calculating the maximum value of the flexural and torsional moments applied on the axle, as well as the relevant coefficients [10]. Consequently, for this axle, the selected shaft diameter is suitable.

2.1.2.2. Calculation in terms of the strength

The maximum shear stress theory controls the design of axles made of ductile materials based on their strength. Equations related to the normal and tangential stresses on the cross-section of the hollow axle are as follows [10]:

$$\sigma_b = \frac{32 M_b d_o}{\pi (d_o^4 - d_i^4)} \qquad (5)$$

$$\tau_t = \frac{16 T d_o}{\pi (d_o^4 - d_i^4)} \qquad (6)$$

If there are flexural and torsional moments in an axle, all stresses would be investigated using the stress criterion of σ_V. The benchmark stress based on the theory of the maximum deformation energy is equal to [10]:

$$\sigma_V = \sqrt{\sigma_b^2 + (\alpha_0 \tau_t)^2} \qquad (7)$$

After calculating the flexural and torsional stresses through (5) and (6) and obtaining Bach ratio through [10], σ_V according to the above equation was calculated as $3.0235 \frac{MN}{m^2}$. These stress compared with the yield stress of an axle made of steel E335 with the yield stress of $285 \frac{MN}{m^2}$ is significantly smaller, and thus the axle is adequately sustainable.

2.1.2.3. The critical speed of axles

In the design of axles, the critical speed is an essential parameter in determining the operating speed of axles. All rotating axles, even in the absence of external forces, at the time of rotation, would be deformed. Considering this deformation as a function of speed, it can be stated that the maximum deformation occurs at a speed known as the critical speed. Here, the critical speed is calculated using the methods of the Rayleigh-Ritz and Dunkerley.

For axles on which only one mass is mounted, if the weight of axle as compared with that of the mass is small, the critical speed can approximately be calculated via the Rayleigh-Ritz equation as [11]. For axles with a negligible mass that bear several masses, the initial critical speed is approximately equal to [11]:

$$\omega_c = \sqrt{g \sum_1^j w_n \delta_n \Big/ \sum_1^j w_n \delta_n^2} \qquad (8)$$

To estimate the initial critical speed of an axle with a considerable mass or full load, (8) can be used so that the extensive mass divides into masses m_1, m_2, and m_3, and the weight of each mass would be considered as a point in its gravity center.

Using SolidWorks software and according to the described method, bar and four discs mounted on were divided into four parts; after putting the weight of each section in its mass center, the amount of movement in the mass center of any part would be determined by the software.

On the other hand, the weight of each disc and the total weight of the axle are $340\ N$ and

$520\ N$, respectively. By dividing the axle into four parts; thus, there is for each:

$$w_1 = w_2 = w_3 = w_4 = 470 \qquad (9)$$

Also, given the equality of all w_n (8), the critical speed of axle would be equal to $83886 rpm$.

To approximate the critical speed for a multi-mass system, Dunkerley's equation is used as follows [11]:

$$\frac{1}{\omega_c^2} = \frac{1}{\omega_1^2} + \frac{1}{\omega_2^2} + \frac{1}{\omega_3^2} + \cdots \qquad (10)$$

Where ω_c is the initial critical speed of the multi-mass system. Moreover, ω_1 is the critical speed in the case that there is only one mass, and ω_2 is the critical speed in the presence of two masses.

In this method; using the SolidWorks software, the static displacement of the axle is calculated in the presence of every mass; using the equation $\omega_c = \sqrt{\frac{g}{\delta}}$, the critical speed is calculated in the presence of each mass; and at the end, using Dunkerley's equation, the critical speed of axle is achieved equal to $52410.5\ rpm$.

2.1.2.4. Comparison of the obtained critical and operational speeds of the axle

The axle operational speed is calculated according to the specifications of the engine, including the output power and moment [1] through the following equation:

$$\omega_{shaft} = \frac{p_{motor}}{T_{motor}} \times \frac{r_{small\ wheel}}{r_{shaft}} \qquad (11)$$

Accordingly, the operating speed based upon (11) equals to $349.49 rpm$. As can be seen, the axle critical speed gained by both methods is significantly higher than the axle operational speed.

It should be noted that both Rayleigh-Ritz and Dunkerley equations result in an approximation of the initial regular frequency of vibration, which is assumed to be very close to the critical speed. In general, the Rayleigh-Ritz equation overestimates, and Dunkerley equation underestimates the actual value of the regular

frequency. Calculations show that the critical speed of axle driven by both methods is significantly higher than the operating speed of axle.

2.1.3. Force mechanism

To apply the force at the contact point between two discs, the power screw and nut mechanism are used. Nut displacement provides the possibility for the disc to be attached to the engine in order to push on the central disc. Plastic washers are used to avoid clearance and corrosion on the junction place.

2.1.3.1. Designing the power screw for the force transfer mechanism

In simple screw joints in which screws, nuts, as well as parts are not affected by large forces, and perhaps the loss of pressure in connections is of much importance, accurate calculations are needed. To select a screw, various factors must be taken into consideration, such as profile type of gear, the number of string rounds around the cylinder, the form of the screw head, and screw material. Here, the desired screw is of no-head screw type, i.e., metric screw.

Strong screws are made of steel. Power and moving screws are mainly made of E295 (St 50-2) or E335 (St60-2). In making screws and nuts, the material used in one should be taken into consideration in the other.

2.1.3.2. Calculating the diameter of the moving screws

If the free length of screws as compared to their effective diameter is higher, then applying force would likely cause deformation along the screw that is called buckling. The inner diameter of the screw, therefore, is obtained according to the Euler formula as follows [10]:

$$d_1 \geq \sqrt[4]{\frac{20 F \mathcal{V} \ell_k^2}{E \pi^2}} \tag{12}$$

Where ℓ_k is the effective length which is equal to [10]:

$$\ell_k = 0.7 \times L \tag{13}$$

Where $\mathcal{V}$ is the confidence coefficient with a value between 8 to 10 [10].

According to (12), the diameter of the screw is calculated to be 6 mm.

Now, the appropriate screw would be chosen [10] using the standard tables related to the trapezoidal screws based on DIN103-1. A screw of $Tr\ 20 \times 4$ with the following characteristic seems to be appropriate:

- Outer diameter: 20 mm

- Internal diameter: 15.5 mm

- The side diameter: 18 mm

- Step screw: 4 mm

- Depth of thread: 2.25 mm

- Width of the gear foot: 1.33 mm

In the dynamic state and with respect to the dynamic analysis done by the SolidWorks software, the force swing along the screw axle reaches up to 10 kN. By substituting this value in the above equation, the minimum diameter of 13 mm would result. However, the selected diameter is also higher than this value.

To evaluate the durability and reliability, it should be noted that the used material in making power transmissions screw, which is also known as spindle screw, is the non-alloy structural steel being applied in machining with the yield stress 335 $\frac{N}{mm^2}$ based on DIN EN 10025. The cross-section of the spindle is subject to the tensile or compressive stress, as well as the torsional stress due to the torsional moment. These stresses may be calculated by the following equations [10]:

$$\sigma = \frac{F_A}{A_K} \tag{14}$$

$$\tau_t = \frac{T}{W_t} \tag{15}$$

$$T = F_A \tan(\alpha + \rho_G) r_2 \tag{16}$$

$$\tan \alpha = \frac{p}{d_2 \pi} \tag{17}$$

$$\tan \rho_G = \frac{\mu_G}{\cos \beta_N} \tag{18}$$

To investigate the stability of screw, both stresses are summarized in one stress [10]:

$$\sigma_V = \sqrt{\sigma^2 + 3\tau_t{}^2} \qquad (19)$$

The value for this stress, which is also called the compound stress, should be less than the allowable stress of screws, i.e. σ_{zul} . After calculations, finally, σ_V according to (19) is equal to 2.915 $\frac{N}{mm^2}$, which is less than $\sigma_{zul} = 83.75 \frac{N}{mm^2}$ [10].

On the other hand, the power transmissions screws, which are subject to the compressive stress, should also be tested to avoid buckling. For this purpose, the following equation is suggested [10]:

$$\sigma_p = \frac{F_A p}{m d_2 \pi H_1 k} \qquad (20)$$

Pressure on the sides of the threads should be less than the allowable pressure P_{zul} [10]. According to (20), the pressure on the thread sides is equal to 1.1789 $\frac{N}{mm^2}$ that is less than the value of P_{zul} for E335, i.e. 500 $\frac{N}{mm^2}$.

According to calculations, it is revealed that the power transmission of the intended screw is stable enough to meet all the design requirements.

2.2. Modeling electromechanical slip control simulator in SolidWorks software

According to the mentioned design process and the parameters determined, the electromechanical simulator of slip control in SolidWorks software is developed. The side and top views of this simulator in the SolidWorks software are shown in figure 1.

Now, by obtaining the simulator dynamic equations and solving them, the dynamic phenomenon of slip is modeled.

3. Dynamic Modeling of Slip Phenomenon

3.1. Slip mechanism of the wheel for trains

The traction mechanism of railway trains can be modeled as follows [12]:

$$F_a = \mu(\xi)N \qquad (21)$$

$$\xi = \frac{r\omega - v}{v} \qquad (22)$$

In this equation, the adhesion force F_a is the same friction force that is perpendicular to the normal one. This force depending on the relative speed between wheel and rail can be desirable or undesirable. Adhesion force F_a with respect to the adhesion coefficient $\mu(\xi)$ changes, this depends upon the slip ratio ξ, road conditions, axial load, and the initial braking speed, i.e., the speed at which the braking action starts. Figure 2 shows the dependence of the adhesion coefficient $\mu(\xi)$ to the slip ratio of ξ and rail conditions [12].
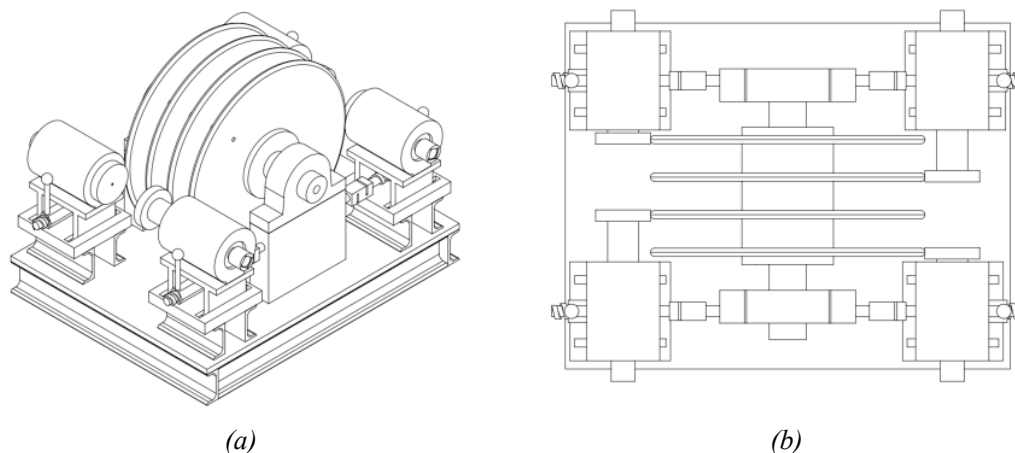

(a)   *(b)*

Figure 1. Electromechanical simulator of slip control in SolidWorks software: (a) Side view; (b) Top view
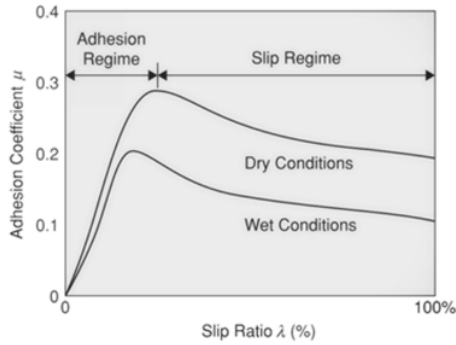
Figure 2. Dependence of the adhesion coefficient $\mu(\xi)$ to the slip ratio of ξ and rail conditions [12]

3.2. Linear and nonlinear creep models and the adhesion force

According to the Kalker theory [13], creep in longitudinal, transverse, and rotational directions can be calculated via the following formulas:

$$\xi_x = \frac{V_{xw} - V_{xr}}{V} \tag{23}$$

$$\xi_y = \frac{V_{yw} - V_{yr}}{V} \tag{24}$$

$$\xi_{sp} = \frac{\omega_w - \omega_r}{V} \tag{25}$$

Longitudinal and transverse adhesion forces, as well as creep rotational moment for the linear model, can be calculated through the following formulas [13]:

$$F_x = f_{110}\xi_x \tag{26}$$

$$F_y = f_{220}\xi_y + f_{230}\xi_{sp} \tag{27}$$

$$M_z = -f_{230}\xi_y + f_{330}\xi_{sp} \tag{28}$$

Also, the creep coefficients can be obtained through the following equations [13]:

$$f_{110} = abGC_{11} \tag{29}$$

$$f_{230} = (ab)^{3/2} GC_{23} \tag{30}$$

$$f_{330} = (ab)^2 GC_{33} \tag{31}$$

$$f_{220} = abGC_{22} \tag{32}$$

So that

$$G = 2G_w G_r/(G_w + G_r) \tag{33}$$

Thus, considering the nonlinear creep model, longitudinal and transverse adhesion forces, as well as creep rotational moment, can be calculated from the following expressions [13]:

$$F_x' = \varepsilon F_x \tag{34}$$

$$F_y' = \varepsilon F_y \tag{35}$$

$$M_z = -f_{23}\xi_y + f_{33}\xi_{sp} \tag{36}$$

Hence, $x, y, and\ z$ indicate the coordinates of the contact point, where F_x and F_y are derived from the following equations [13]:

$$F_x = f_{11}\xi_x \tag{37}$$

$$F_y = f_{22}\xi_y + f_{23}\xi_{sp} \tag{38}$$

Coefficients can be obtained through the following equations [13]:

$$f_{11} = (N/N_o)^{2/3} f_{110} \tag{39}$$

$$f_{23} = (N/N_0)f_{230} \tag{40}$$

$$f_{22} = (N/N_0)^{2/3}f_{220} \tag{41}$$

$$f_{33} = (N/N_o)^{4/3}f_{330} \tag{42}$$

Besides, the coefficient of the adhesion force can be obtained from the following equations [13]:

$$\tag{43}$$

$$\varepsilon = \begin{cases} \dfrac{\mu N}{F_R}\left[\left(\dfrac{F_R}{\mu N}\right) - \dfrac{1}{3}\left(\dfrac{F_R}{\mu N}\right)^2 + \dfrac{1}{27}\left(\dfrac{F_R}{\mu N}\right)^3\right], F_R \le 3\mu N \\ \dfrac{\mu N}{F_R} \qquad\qquad F_R > 3\mu N \end{cases}$$

So that

$$F_R = \sqrt{F_X^2 + F_Y^2} \tag{44}$$

3.3. Creep equations and the adhesion forces for the simulator

According to the equations presented in the previous section, the creep equations for discs 1

to 4 of the electromechanical simulator are calculated as follows:

$$\xi_{x_i} = \frac{r\omega_{w_i} - R\omega_{r_i}}{R\omega_{r_i}} \quad i = 1,2,3,4 \tag{45}$$

Also, the equivalent creep force is as follows:

$$F_R = \sqrt{F_X^2 + F_Y^2} = F_X \tag{46}$$

Along these lines, the creep forces of the wheels and rail (large and small discs) are calculated as follows:

$$F_{x_i} = \left(N_i / N_0\right)^{2/3} K \xi_{x_i}, i = 1,2,3,4 \tag{47}$$

So that

$$K = abGC_{11} \tag{48}$$

Thus, coefficients of adhesion forces for the wheels and rail can be calculated from the following equations:

$$\varepsilon_i = \begin{cases} \frac{\mu N_i}{F_{x_i}} \left[\left(\frac{F_{x_i}}{\mu N_i}\right) - \frac{1}{3}\left(\frac{F_{x_i}}{\mu N_i}\right)^2 + \frac{1}{27}\left(\frac{F_{x_i}}{\mu N_i}\right)^3 \right], F_{x_i} \leq 3\mu N_i \\ \frac{\mu N}{F_{x_i}} \quad\quad\quad F_{x_i} > 3\mu N_i \end{cases} \tag{49}$$

According to the above equations, the adhesion force between wheel and rail is calculated from the following equation:

$$F_{a_i} = \varepsilon_i F_{x_i} \quad i = 1,2,3,4 \tag{50}$$

4. Dynamic Equations of Wheel and Rail in the Simulator

Dynamical equations of wheels (small discs) and rail (large discs and shafts) are as below.

The dynamic equation of wheels:

$$J_{w_i} \frac{d\omega_{w_i}}{dt} = T_{M_i} - r_{w_i}F_{a_i}, \ i = 1,2,3,4 \tag{51}$$

$$J_{w_i} \ddot{\theta}_i = T_{M_i} - r_{w_i}F_{a_i}$$

The dynamic equation of rail:

$$J_{eq} \frac{d\omega_5}{dt} = F_{a_1} \times R_1 + F_{a_2} \times R_2 + F_{a_3} \times R_3 + F_{a_4} \times R_4 - c\omega_5 \tag{52}$$

$$J_{eq} \ddot{\theta}_5 = F_{a_1} \times R_1 + F_{a_2} \times R_2 + F_{a_3} \times R_3 + F_{a_4} \times R_4 - c\dot{\theta}_5$$

4.1. State equations of wheel and rail in the simulator

The dynamic equations in the previous section are used to determine the state equations of wheel and rail; these equations are presented as follows:

$$\tag{53}$$

$$\begin{cases} \dot{x}_1 = x_2 \\ \dot{x}_2 = T_{M_1}/J_{w_1} - \frac{r_{w_1}F_{a_1}}{J_{w_1}} \\ \dot{x}_3 = x_4 \\ \dot{x}_4 = T_{M_2}/J_{w_2} - \frac{r_{w_2}F_{a_2}}{J_{w_2}} \\ \dot{x}_5 = x_6 \\ \dot{x}_6 = T_{M_3}/J_{w_3} - \frac{r_{w_3}F_{a_3}}{J_{w_3}} \\ \dot{x}_7 = x_8 \\ \dot{x}_8 = T_{M_4}/J_{w_4} - \frac{r_{w_4}F_{a_4}}{J_{w_4}} \\ \dot{x}_9 = x_{10} \\ \dot{x}_{10} = \frac{F_{a_1} \times R_1}{J_{eq}} + \frac{F_{a_2} \times R_2}{J_{eq}} + \frac{F_{a_3} \times R_3}{J_{eq}} + \frac{F_{a_4} \times R_4}{J_{eq}} - \frac{cx_{10}}{J_{eq}} \end{cases}$$

5. Results of Solving Equations without a Controller

Simulation is done in 200s with solver ODE 45 in Simulink. Initial angular speeds for each of the four small discs is 0 rad/sec ; for the large discs and the main axle is 1 rad/sec. Moreover, the friction coefficient is 0.3, the radius of small and large discs are selected as 0.06 m and 0.3m. Then, a torque of 1 N.m is applied on the first disc; results are shown in figures 3 and 4.

As can be observed in figure 3, the chart of angular velocity is the same for all four small discs. This is due to the same conditions of contact and friction coefficient for all four discs. Another significant point is that up to approximately 100 seconds is needed to reach a steady-state and get stable system performance practically. The reason for this delay is the small
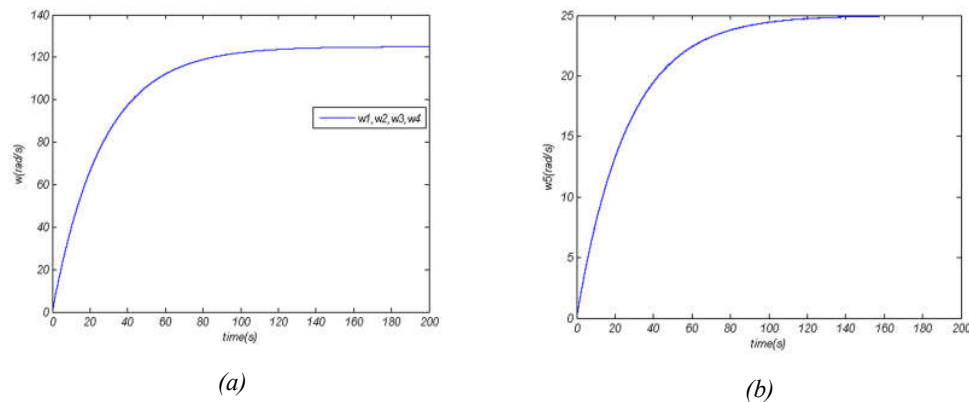
(a)   *(b)*

Figure 3. Angular velocity discs (a) small discs (b) large disc

area of adhesion between small and large discs at the beginning of the contact. The purpose of controlling such a system, therefore, is to reduce the hundred-second time interval so that the system becomes stable quickly as possible.
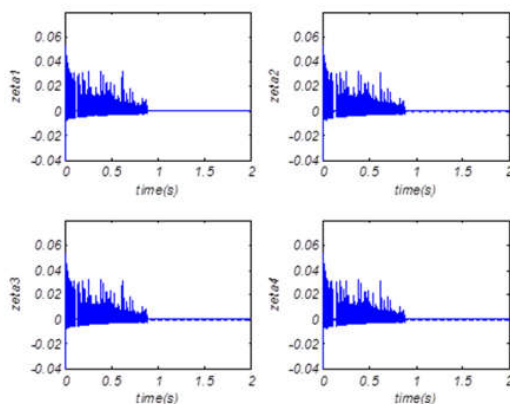

Figure 4. The slip ratio

From this graph, it is also evident that the angular velocity of small discs is stable around $120 \frac{rad}{sec}$; however, the large disc velocity tends to $24 \frac{rad}{sec}$. This ratio is equal to that of small to large disc radius ($\frac{r}{R} = \frac{1}{5}$), which indicates the simulation result is correct. Besides, there are very few variations in velocity curves due to the micro slip in the contact area between the two discs (figure 4).

6. Active Control of the Simulator

In this section, a fuzzy controller is added to the model presented in the previous section. The reason for using this system is that it is intuitive and can easily be written through intuition. Three controlling mechanisms are employed to select the best method:

1- Fuzzy control method for all axles of a wagon (per vehicle),

2- Fuzzy control method for each bogie (per bogie),

3- Fuzzy control method for each axle (per wheelset).

In this fuzzy control system, the triangular membership function is utilized. The fuzzy rules set are written based on the work of Frylmark and Johnsson [14]. The controlling surface of the fuzzy controller in terms of written rules is as follows:
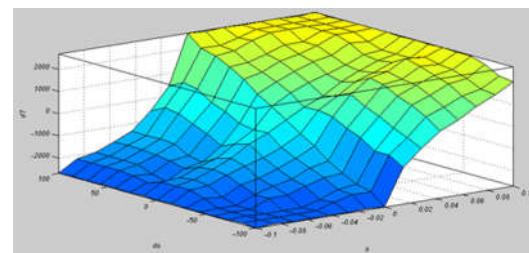

Figure 5. Control surface of fuzzy controller

7. The Results of Control Methods for the Slip Simulator

Three different types of motion trends are considered for simulation, and results for all control methods are presented.

7.1. First simulation and its results

In this simulation, it is considered to have initial angular speeds for all axles equal to 90 $\frac{rad}{sec}$, the initial angular speed of rail (large discs and the main shaft) equal to 12 $\frac{rad}{sec}$, the coefficient of friction between the wheels and rail for all wheels equal to 0.3, and the radius of all wheels equal to $0.06\ m$.

The results are shown in figures 6 and 7.

7.1.1. Interpretation of the first simulation results

As is clear from figures 6 and 7, slipping in the second of 13 has reached to a small value. The difference in the results of the three controlling mechanisms, i.e., for all axles, each bogie, as well as each axle, is not considerable.

It was also observed that considering the control algorithm, the large disc velocity representing the linear velocity of the locomotive is nearly $720 \frac{rad}{sec}$; while without considering the controller, its value is $24\frac{rad}{sec}$.

7.2. The second simulation and its results

The condition is exactly similar to the first stimulation. Only the radius of the third and fourth axles is $4\ mm$ less. This case is similar to the case in which one of the bogies of locomotives has been abandoned and replaced with a newer bogie due to a technical problem. Therefore, the new bogie wheels radius varies with the others due to less work and wear.
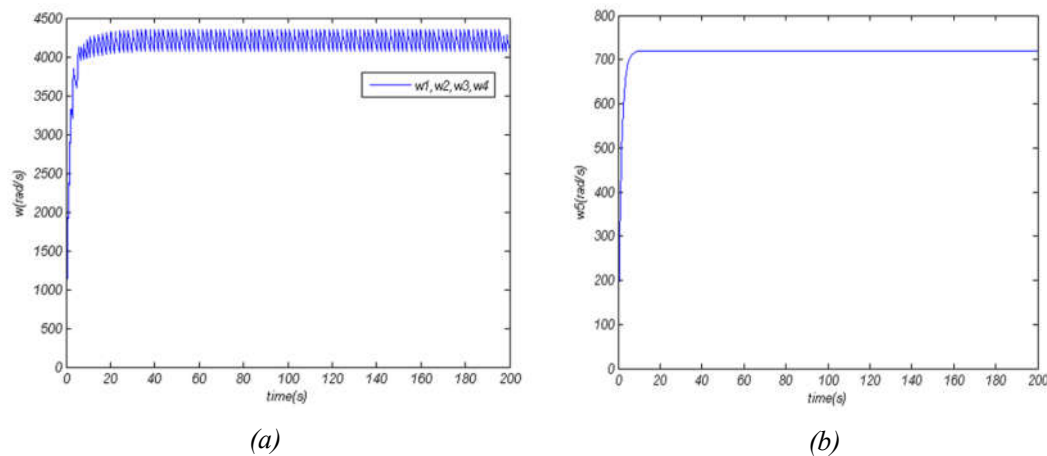

(a)   *(b)*

Figure 6. Angular velocity of discs for the first controlling mechanism (a) Small discs (b) Large disc
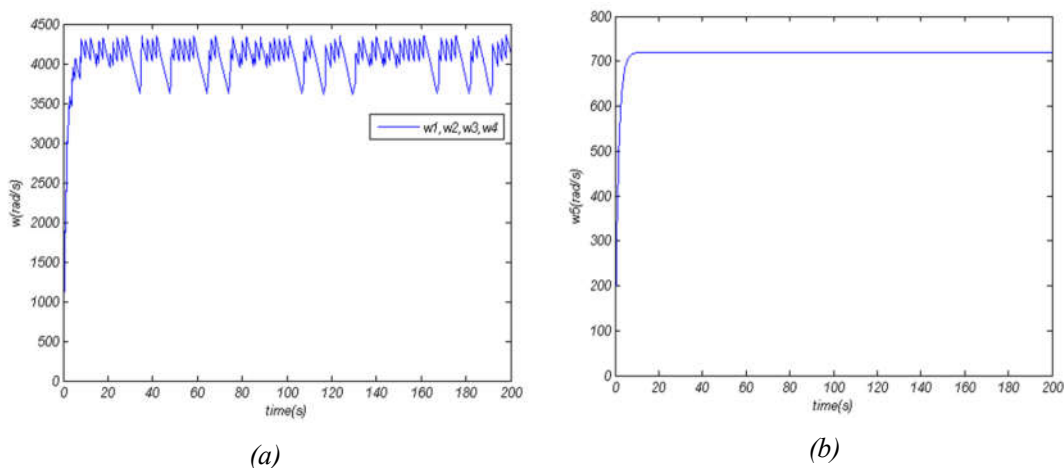

(a)   *(b)*

Figure 7. Angular velocity of discs for the second and third controlling mechanism (a) Small discs (b) Large disc

The results are shown in figures 8 and 9.

7.2.1. Interpretation of the second simulation results

As can be seen in figure 8, in the simulation with the control mechanism for all axles, the third and fourth axles begin to slid; while in simulation with two other control mechanisms, it does not happen (figure 9). The reason is that in the control mechanism for all axles, only one control signal is issued to control all four axles. In this method, indeed, the adhesion force F_a is read in all four axles, and control is applied to the least amount of force, and eventually, the produced signal is sent to all four axles. However, it may be predictable that if an axle of four-axle locomotives is replaced with a new one, due to a change of a new axle radius with old ones, the control mechanism does not work

for each bogie and cannot control the slip of four axles. The limitation of this control method is shown in the next section.

7.3. The third simulation and its results

In this simulation, conditions are similar to the first except that the coefficient of friction for the fourth axle is 0.2. This is like the case in which because of low friction coefficient between wheel and rail, sandblasting device of four-axle locomotives begin to work and increase the friction coefficient by sprinkling sand on the rails. However, since the operation cannot be performed for each axle, it is entirely possible to have the friction coefficient of an axle less than other topics. The results are shown in figures 10 and 11.
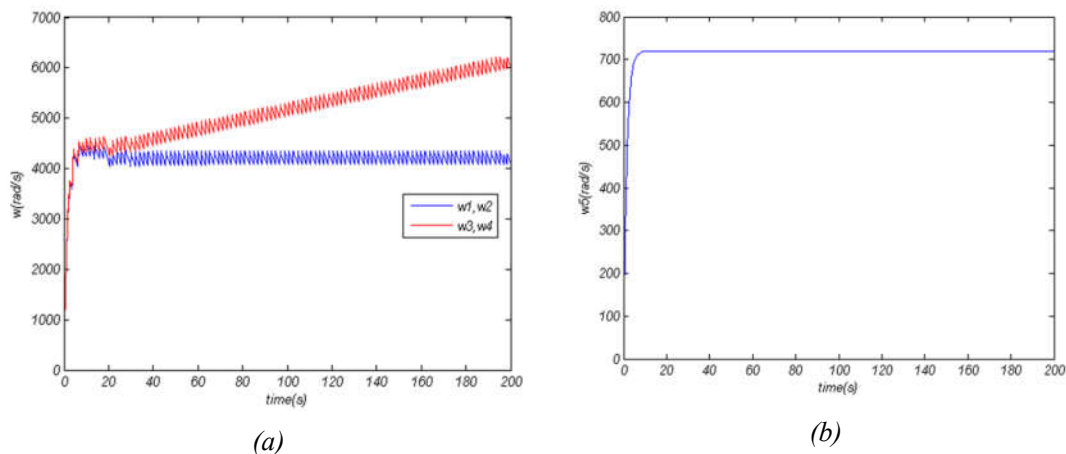

Figure 8. Angular velocity of discs for the first controlling mechanism (a) Small discs (b) Large disc
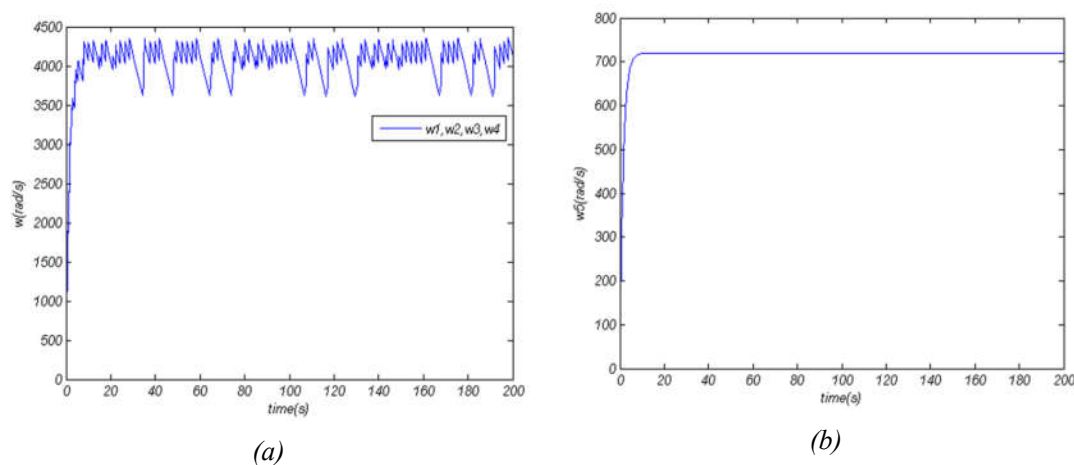

Figure 9. Angular velocity of discs for the second and third controlling mechanism (a) Small discs (b) Large disc
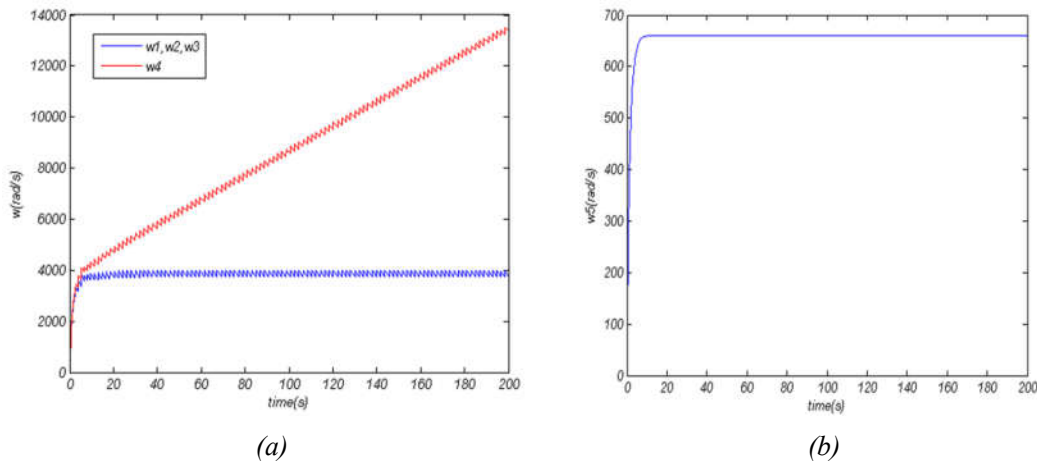
(a)   *(b)*

Figure 10. Angular velocity of discs for the first and second controlling mechanism

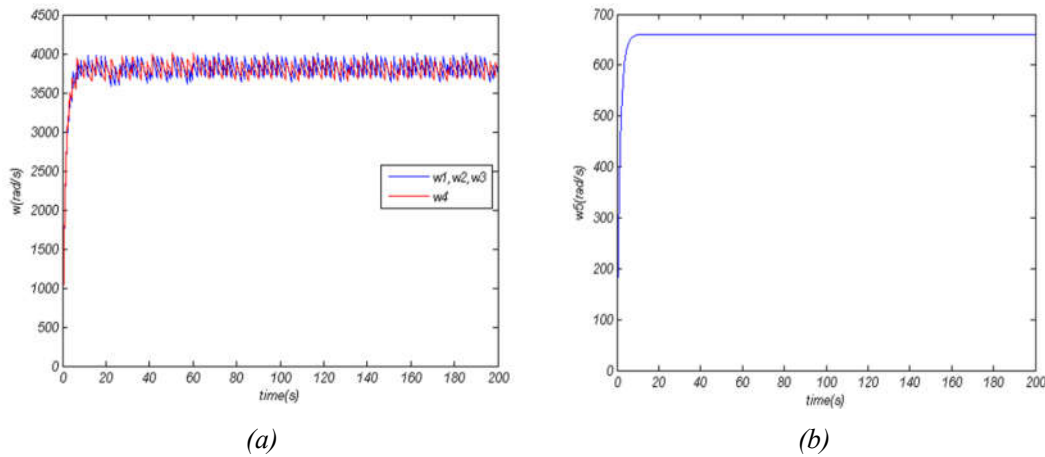(a) Small discs (b) Large disc

(a)   *(b)*

Figure 11. Angular velocity of discs for the third controlling mechanism (a) Small discs (b) Large disc

7.3.1. Interpretation of the third simulation results

As can be seen, the best performance is for the third control mechanism. As shown in Figure 11, despite a change in friction coefficient and its reduction for the fourth wheel, the wheel is not slipping, and control mechanisms maintain adhesion between wheel and rail in the highest possible value by changing the input torque. Furthermore, it can be seen from Figures 10 and 11 that large disc velocity is less than other states and gets around $660 \frac{rad}{sec}$; this can be due to reducing the friction coefficient of one of the discs.

7.4. Investigation of the results' Accuracy

In order to verify the results obtained, the exact solution (52) is used. In this formula, F_{a_1}, F_{a_2}, F_{a_3} , and F_{a_4} are adhesion forces between wheel and rail; the greatest amount of these forces is equal to $\mu_i N_i$. Therefore, when their amount all is equal to $\mu_i N_i$, the highest possible adhesion between wheels and rails, and thus the most velocity is achieved. Now, by putting values $\mu_i N_i$ instead of F_{a_i} , maximum velocity is measured.

$$J_{eq}\frac{d_{\omega_5}}{dt} = \mu_1 N_1 R_1 + \mu_2 N_2 R_2 \quad (54)$$
$$+ \mu_3 N_3 R_3$$
$$+ \mu_4 N_4 R_4 - c\omega_5$$

Finally, by solving the above equation and assuming the initial condition ω_0, the most velocity of the large disc can be obtained as follows:

$$\omega_5 = \frac{\sum_{i=1}^4 \mu_i N_i R_i}{c} \quad (55)$$
$$- \frac{(\sum_{i=1}^4 \mu_i N_i R_i - c\omega_0)}{c} e^{-\frac{ct}{J_{eq}}}$$

Considering the steady-state conditions, the second term of the above equation is zero; later, the following equation can be obtained for a maximum velocity of large disc:

$$\omega_5 = \frac{\sum_{i=1}^4 \mu_i N_i R_i}{c} \quad (56)$$

Ultimately, by substituting the respective values in (56), the maximum speed of the large disc is $720 \frac{rad}{sec}$ that is consistent with the results obtained. Also, in the case that the fourth wheel friction coefficient was assumed 0.2, the value $660 \frac{rad}{sec}$ can be obtained through the above equation for the maximum speed of the large disc, which is in accordance with the results of the previous section.

8. Conclusions

In this paper, after investigation of adhesion phenomena and factors affecting it, certain methods and strategies of slip control systems were briefly studied. Then, given the importance of the anti-slip systems, the electromechanical device of testing such systems was introduced and designed to assess the performance of control systems. A simulation, based on the dynamic equations of this device, indicates that it can simulate real terms of wheel and rail contact in a laboratory setting. Thus, it can be concluded that the proposed model can be used to study the slip control algorithm in modern four-axle locomotives. Further, various slip control mechanisms were studied, taking into account the three different processes of motion for four-axle locomotives. Finally, it was determined that the best performance could be achieved in terms of slip control between wheel and rail by controlling each axle locomotives individually.

List of Symbols

Bearing lifetime	L
Expected average lifetime	L_h
Dynamic transmission coefficient	C
Equivalent load of bearing	P
Radial coefficient dependent to the ratio of the effective axial force on the effective radial force	x
Axial coefficient to calculate the axial force	y
Temperature factor	f_t
Lifetime factor	f_L
The factor of the number of rounds	f_n
Outside diameter of axle	d_o
Inner diameter of axle	d_i
Maximum bending moment	M_b
Maximum torsional torque	M_t
Ratio of internal to external diameter	K
Combined shock and fatigue factor applied to the bending moment	k_b
Combined shock and fatigue factor applied to the bending moment	k_t
Largest bending or torsional moments at the endangered cross section, considering strikes and loading peaks	S_s
Compound stress	σ_v
Bending stress	σ_b
Torsional stress	τ_t
Bach ratio	α_0
Weight of the nth mass in the Rayleigh Ritz method	w_n
Static deformation in the place of the nth mass in Rayleig	δ_n

Ritz method		Rotational creep	ξ_{sp}
Total number of masses in Rayleigh Ritz method	j	Longitudinal adhesion force	F_x
Constant of gravity	g	Transverse adhesion force	F_y
Critical speed	ω_c	Creep rotational moment	M_z
Tensile or compressive force of moving screw	F	Creep coefficients	f_{ij}
Length of screw affecting by the buckling	ℓ_k	Semiaxis of the contact ellipse in the rolling direction	a
Length of screw	L	Semiaxis of the contact ellipse in the lateral direction	b
Confidence coefficient	ν	Modulus of rigidity	G
Inner diameter of the screw	d_1	Creepage and spin coefficients	C_{ij}
Young's modulus	E	Nonlinear longitudinal adhesion force	F'_x
Tensile or compressive stress of moving screw	σ	Nonlinear transverse adhesion force	F'_y
Longitudinal force of the screw	F_A	Coefficient of adhesion force	ε
Cross section of the screw's core	A_K	Normal force	N_0
Torsional stress in the screw	τ_t	Instantaneous normal force	N
Torsional torque applied to the screw	T	Resultant force	F_R
Cross-sectional module of the cross section of the screw's	W_t	Small disc moment of inertia	J_{w_i}
Core against torsion		Small disc radius	r_{w_i}
Thread pitch angle	α	Torque of motor	T_{M_i}
Friction angle of the thread	ρ_G	Equivalent moment of inertia	J_{eq}
Thread pitch	p	Large disc radius	R_i
Diameter of the thread's side	d_2	Damping factor	c
Coefficient of friction in thread	μ_G		
Side angle of screw in the normal cross section	β_N		
Pressure on the thread's sides	σ_p		
Height of thread	H_1		
Transport coefficients of thread	k		
Adhesion force	F_a		
Adhesion coefficient	$\mu(\xi)$		
Slip ratio	ξ		
Longitudinal creep	ξ_x		
Transverse creep	ξ_y		

References

[1] W.-S. Kim, Y.-S. Kim, J.-K. Kang, S.-K. Sul, Electro-mechanical re-adhesion control simulator for inverter-driven railway electric vehicle, in Proceeding of IEEE, (1999), pp. 1026-1032.

[2] T.X. Mei, J.H. Yu, D.A. Wilson, A mechatronic approach for anti-slip control in railway traction, IFAC Proceedings Volumes, Vol. 41, Issue 2, (2008), pp. 8275-8280.

[3] D.-H. Hwang, M.-S. Kim, D.-Y. Park, Y.-J. Kim, D.-H. Kim, Re-adhesion control for high-speed electric railway with parallel motor

control system, in Proceeding of IEEE, (2001), pp. 1124-1129.

[4] W. Zhang, J. Chen, X. Wu, X. Jin, Wheel/rail adhesion and analysis by using full scale roller rig, Wear, Vol. 253, No. 1, (2002), pp. 82-88.

[5] H.-O. Yamazaki, Y. Karino, M. Nagai, T. Kamada, Wheel slip prevention control by sliding mode control for railway vehicles (experiments using real size test), in Proceeding of IEEE, (2005), pp. 271-276.

[6] J. Huang, J. Xiao, H. Weiss, Simulation study on adhesion control of electric locomotives based on multidisciplinary virtual prototyping, in Proceeding of IEEE, (2008), pp. 1-4.

[7] D. Smejkal, M. Omasta, M. Hartl, An experimental investigation of the adhesion behavior between wheel and rail under oil, water and sanding conditions, in: Modern Methods of Construction Design, Eds., Springer, (2014), pp. 623-628.

[8] N. Bosso, A. Gugliotta, N. Zampieri, Strategies to simulate wheel–rail adhesion in degraded conditions using a roller-rig, Vehicle System Dynamics, Vol. 53, No. 5, (2015), pp. 619-634.

[9] M. Naeimi, Z. Li, R. Dollevoet, Preliminary results on dynamic analysis of a new test rig for wheel-rail contact series, International Journal of Railway Research, Vol. 3 , No. 2, (2016), pp. 9-19.

[10] J.E. Shigley, C.R. Mischke, R.G. Budynas, X. Liu, Z. Gao, Mechanical Engineering Design: McGraw-Hill New York, (1989).

[11] A.S. Hall, A.R. Holowenko, H.G. Laughlin, Theory and Problems of Machine Design: McGraw-Hill, (1961).

[12] S.H. Park, J.S. Kim, J.J. Choi, H.-o. Yamazaki, Modeling and control of adhesion force in railway rolling stocks, Control Systems, IEEE, Vol. 28, No. 5, (2008), pp. 44-58.

[13] R.V. Dukkipati, J.R. Amyot, Computer-aided simulation in railway dynamics, Mechanical Engineering; 61-Untraced Series, No. 61, (1988).

[14] D. Frylmark, S. Johnsson, Automatic slip control for railway vehicles, MSc Thesis, Linköping University, Linköping, Sweden, (2003).